

A comparative study on the catalytic activity of $\text{Fe}_3\text{O}_4@\text{SiO}_2\text{-SO}_3\text{H}$ and $\text{Fe}_3\text{O}_4@\text{SiO}_2\text{-NH}_2$ nanoparticles for the synthesis of spiro [chromeno [2, 3-c] pyrazole-4, 3'-indoline]-diones under mild conditions

Fatemeh Alemi-Tameh¹ · Javad Safaei-Ghomi¹ ·
Mohammad Mahmoudi-Hashemi¹ ·
Raheleh Teymuri²

Received: 14 January 2016 / Accepted: 1 February 2016
© Springer Science+Business Media Dordrecht 2016

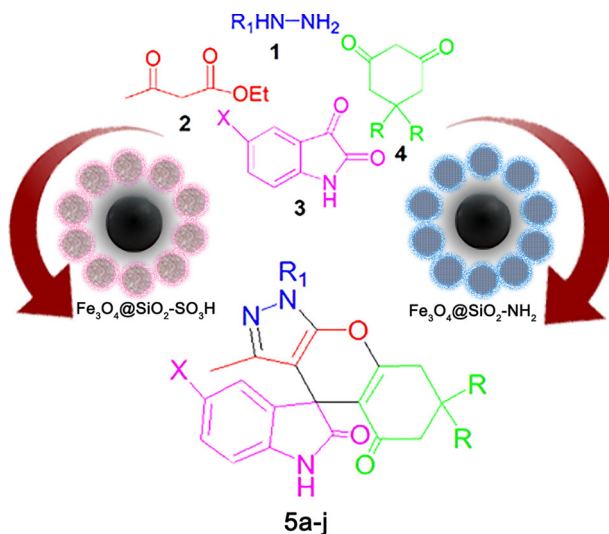
Abstract Sulfuric acid and (3-aminopropyl)-triethoxysilane were successfully attached to the core-shell structure of $\text{Fe}_3\text{O}_4@\text{SiO}_2$ nanoparticles separately. The prepared nanoparticles were characterized by vibrating sample magnetometer, powder X-ray diffraction, scanning electronic microscopy, thermal gravimetric analysis, energy dispersive X-ray spectroscopy, and Fourier transform infrared spectroscopy. To compare the efficiency of the two prepared functionalized magnetic nanoparticles, they were employed as catalysts for the synthesis of spirooxindole containing chromene ring fragments in one-pot four-component reactions. Sulfuric acid-functionalized magnetic nanoparticles showed high catalytic activity in mild reaction conditions and short reaction times and excellent yields of products. The catalyst was easily separated using a magnet and reused for several cycles of reactions without any significant loss of catalytic activity.

✉ Javad Safaei-Ghomi
safaei@kashanu.ac.ir

¹ Department of Chemistry, Science and Research Branch, Islamic Azad University, Tehran, I. R. Iran

² Department of Organic Chemistry, Faculty of Chemistry, University of Kashan, Kashan 51167, I. R. Iran

Graphical Abstract



Keywords $\text{Fe}_3\text{O}_4@\text{SiO}_2\text{-SO}_3\text{H}$ NPs · Spirooxindoles · Multicomponent reactions · One-pot synthesis · Core-shell

Introduction

Following the principles of green chemistry, using recyclable solid catalysts in organic reactions has attracted much attention in recent years [1]. Among different solid catalysts, supported magnetic nanoparticles (MNPs) are more interesting and widely used in organic reactions [2]. MNPs have especially attracted great attention due to their extensive range of usages in different fields such as drug delivery [3], magnetic resonance imaging (MRI) [4], cancer treatment through hyperthermia [5], and absorption of heavy metals from aqueous solutions [6]. The significant properties of Fe_3O_4 -based nanocatalysts include high stability, easy preparation, high catalyst loading, and simple catalyst recycling. In addition, surface functionalization of MNPs is an effective way to create a link between the feature of homogeneous and heterogeneous catalysis [7, 8]. Recently, MNPs have been used as an efficient heterogeneous nanocatalyst in a number of organic reactions such as Buchwald–Hartwig, Suzuki [9], Sonogashira–Hagihara [10], and Paal–Knorr [11, 12] reactions, synthesis of sulfonamides [13], coupling of phenols with aryl halides [14], and synthesis of α -aminonitriles and imines [15].

Multicomponent reactions (MCRs) are regarded as economic methods for the construction of novel complex molecules in a single step procedure. High atom economy, short reaction times, high selectivity, minimized waste, and avoidance of costly purification processes are the characteristics of MCRs [16, 17]. Using these procedures provide a significant route to produce biologically active compounds [18,

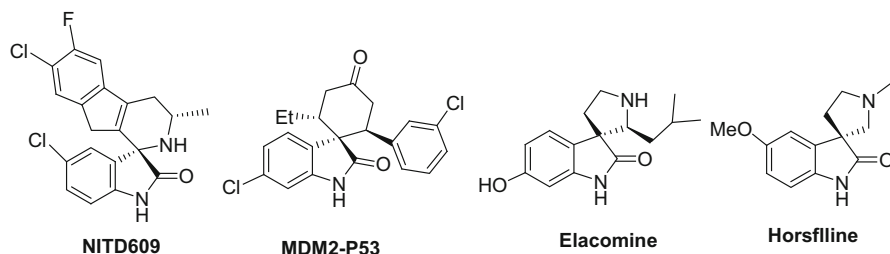


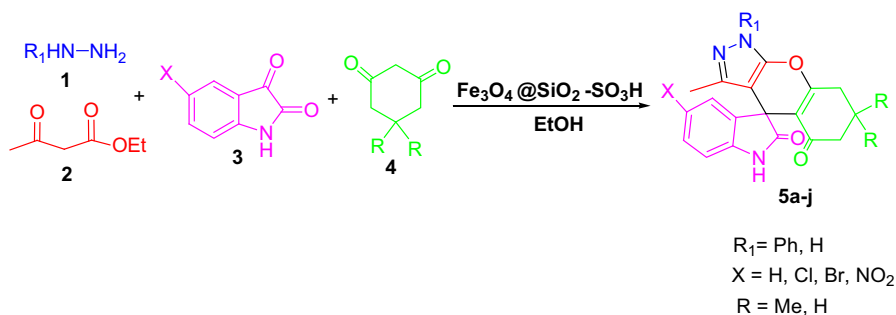
Fig. 1 Some biologically important molecules containing spirooxindole motif

19]. The indole nucleus is a renowned heterocyclic unit in a variety of pharmacological agents [20]. Moreover, it has been reported that sharing of indole C-3 in the creation of spiroindolines greatly improved its biological property [21–24]. The spirooxindole system is the core structure of many biologically active molecules such as NITD609 and MDM2-P53 [25], Elacomine and Horsflinone (Fig. 1) [26].

Because of their extensive biological activities, producing novel spirooxindole derivatives is an interesting subject in medicinal chemistry. Recently, several attempts have also been made for the construction of spirooxindoles via one-pot four-component reactions of isatin, hydrazine hydrate, ethyl acetoacetate, and a compound with an acidic α -hydrogen such as dimedone or malononitrile in the presence of an acid catalyst such as *p*-toluene sulfonic acid [27] or a base catalyst such as 4-dimethylaminopyridine (4-DMAP) [28], meglumine [29], piperidine [30], *L*-proline, and a silica-supported organocatalyst system based on *L*-proline (SSLP) [31]. Although all reports have their own merits, some of these methods have certain drawbacks such as use of toxic, non-reusable, and expensive catalysts, consumption of large amounts of catalyst, long reaction times and high temperatures. Therefore, continuing research to find economical procedures seems to be necessary. In this paper we decided to report an efficient and green method for the synthesis of spiro [chromeno [2, 3-*c*] pyrazole-4, 3'-indoline]-diones via one-pot two-step four-component reaction of isatin, hydrazine hydrate, ethyl acetoacetate, and dimedone or 1, 3-cyclohexadione. Also, we compared sulfuric acid functionalized magnetic nanoparticles and amino functionalized magnetic nanoparticles as acid and base catalysts to promote the yields and rates of this reaction (Scheme 1).

Experimental

All materials were purchased from Sigma–Aldrich and Merck and were used without further purification. All melting points were determined in capillary tubes on a Boetius melting point microscope. ^1H NMR and ^{13}C NMR spectra were recorded on Bruker Avance-400 MHz spectrometer using DMSO-d_6 as solvent. The elemental analyses (C, H, and N) were obtained by means of a Carlo ERBA Model EA 1108 analyzer. Fourier transform infrared (FTIR) spectra were recorded on WQF-510, spectrometer 550 Nicolet in the range of 400–4000 cm^{-1} using KBr pellets. The energy-dispersive X-ray spectroscopy (EDS) measurements were performed by



Scheme 1 One-pot four-component reaction for the synthesis spiro [chromeno [2, 3-c] pyrazole-4, 3'-indoline]-diones derivatives

SAMX analyzer. Powder X-ray diffraction (XRD) measurements were carried out on a Philips diffractometer of X'pert Company with monochromatized Cu K α radiation ($\lambda = 1.54056$ nm). A TGAQ5 thermogravimetric analyzer was used to study the thermal properties of the compounds under an inert N₂ atmosphere at 20 mL min⁻¹ and heating rate of 10 °C min⁻¹. SEM images were taken by MIRA3-TESCAN. The magnetic properties of Fe₃O₄, Fe₃O₄@SiO₂, Fe₃O₄@SiO₂-NH₂, and Fe₃O₄@SiO₂-SO₃H nanoparticles were measured with a vibrating sample magnetometer (VSM, PPMS-9T) at 300 K in Kashan University, Iran.

Preparation of Fe₃O₄ nanoparticles

Fe₃O₄ nanoparticles were synthesized by co-precipitation. FeCl₃·6H₂O (11.68 g) and FeCl₂·4H₂O (4.30 g) were dissolved in 200 mL deionized water, then 15 mL NH₃·H₂O (25 %) was added to the solution drop wise under nitrogen atmosphere and vigorous stirring at 70–75 °C. The magnetic nanoparticles were separated from solution by using an external magnet and washed twice with deionized water.

Preparation of Fe₃O₄@SiO₂ nanoparticles

One gram of magnetic nanoparticles was dispersed in 20 mL ethanol in ultrasonic bath and sonicated for 30 min at room temperature. Then, 6 mL aqueous NH₃ (25 %) and 2 mL tetraethyl orthosilicate (TEOS) were added to the solution. The resulting solution was stirred at 35–40 °C for 24 h. The Fe₃O₄@SiO₂ NPs were separated from solution by using an external magnet and washed with ethanol (3 × 15 mL) and dried at room temperature.

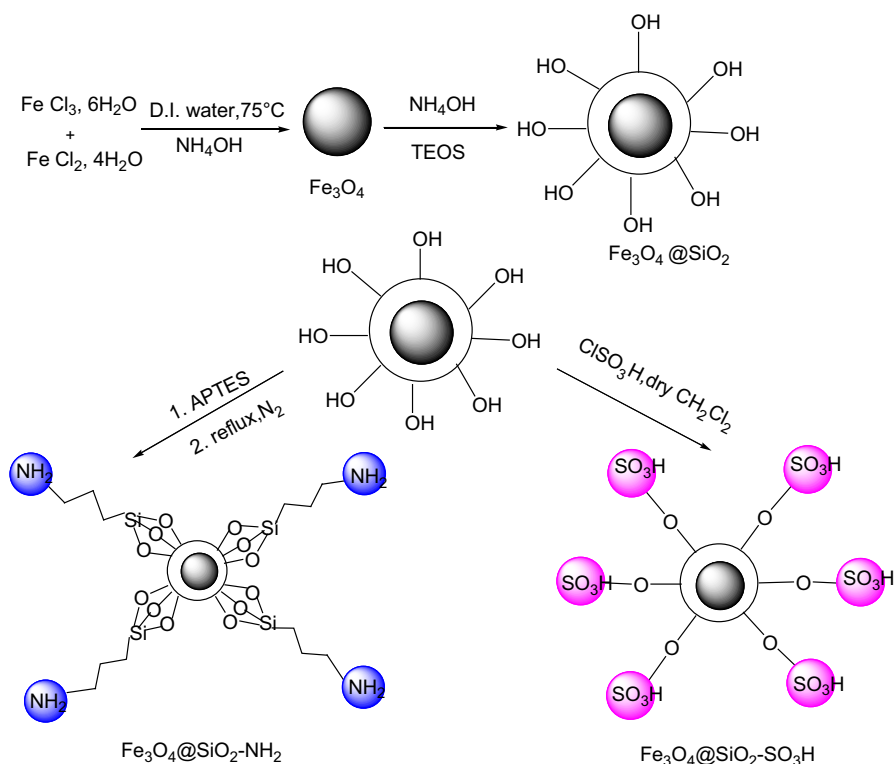
Preparation of Fe₃O₄@SiO₂-NH₂ nanoparticles

One gram of Fe₃O₄@SiO₂ nanoparticles was dispersed in 25 mL of dry toluene and sonicated for 15 min. Then, 2.2 mL 3-(aminopropyl)-triethoxysilane (APTES) was added to the solution drop wise and the mixture was refluxed under nitrogen atmosphere with vigorous stirring for 20 h. Finally, Fe₃O₄@SiO₂-NH₂ nanoparticles

were separated from solution by using a magnet and washed several times with 20 mL ethanol and dried at room temperature. The APTES content in $\text{Fe}_3\text{O}_4@\text{SiO}_2$ NPs is 2.84 mmol/g which agrees well with the content of nitrogen element in $\text{Fe}_3\text{O}_4@\text{SiO}_2\text{-NH}_2$ NPs evaluated by elemental analysis.

Preparation of $\text{Fe}_3\text{O}_4@\text{SiO}_2\text{-SO}_3\text{H}$ nanoparticles

Firstly, 1 g of $\text{Fe}_3\text{O}_4@\text{SiO}_2$ was dispersed in dry CH_2Cl_2 (16 mL) and sonicated for 10 min. Then, chlorosulfonic acid (0.8 mL in dry CH_2Cl_2) was added drop-wise to a cooled (ice-bath) solution of $\text{Fe}_3\text{O}_4@\text{SiO}_2$, during a period of 30 min under vigorous stirring. The mixture was stirred for 60 min, while the residual HCl was removed by suction. The resulted MNPs were separated by using a magnet, washed several times with dried CH_2Cl_2 and methanol before being dried under vacuum at 60 °C. The number of H^+ sites of $\text{Fe}_3\text{O}_4@\text{SiO}_2\text{-SO}_3\text{H}$ NPs was determined by pH-ISE conductivity titration (Denver Instrument Model 270) and found to be 1.69 H^+ sites per 1 g of solid acid at 25 °C. The overall schematic procedure used to synthesize the magnetic nanocatalysis is illustrated in Scheme 2.



Scheme 2 Preparation routes of $\text{Fe}_3\text{O}_4@\text{SiO}_2\text{-NH}_2$ and $\text{Fe}_3\text{O}_4@\text{SiO}_2\text{-SO}_3\text{H}$ nanoparticles

General procedure for the Fe₃O₄@SiO₂-SO₃H NPs catalyzed multicomponent synthesis of spiro [chromeno [2, 3-c] pyrazole-4, 3'-indoline]-diones derivatives (5a–j)

A mixture of hydrazine hydrate 1 (1.1 mmol), ethyl acetoacetate 2 (1.1 mmol), isatin 3 (1 mmol), and Fe₃O₄@SiO₂-SO₃H (0.02 g) nanoparticles was heated in EtOH (10 mL) at 80 °C for 5 min. Then, dimedone 4 (1 mmol) was added to the above mixture, and the mixture was heated for 25 min. The completion of the reaction was monitored by TLC, and the catalyst was separated from reaction by an external magnet before work-up. Then the mixture was poured into cold water and the obtained precipitate was filtered and recrystallized twice in EtOAc/n-hexane (3:1).

Spectral data of products

3, 7, 7-Trimethyl-7, 8-dihydro-1H-spiro [chromeno [2, 3-c] pyrazole-4, 3'-indoline]-2', 5(6H)-diones (5a)

mp 220 °C (dec); IR (KBr): (vmax/cm⁻¹): 3374 (stretch NH), 3182 (stretch NH), 1691 (stretch CO), 1612 (stretch CO). ¹H NMR (CDCl₃, 400 MHz): 0.97 (6H, s, 2CH₃), 1.40 (3H, s, CH₃), 1.90–2.00 (2H, m, CH₂), 2.20–2.30 (2H, m, CH₂), 6.85–6.86 (1H, m, CH), 6.87–6.88 (1H, m, CH), 6.93–6.94 (1H, m, CH), 7.13–7.14 (1H, m, CH), 11.08 (1H, s, NH), 11.72 (1H, bs, NH) ppm. ¹³C NMR (CDCl₃, 100 MHz): δ 11.10, 25.42, 30.50, 42.48, 48.10, 51.82, 97.80, 110.50, 120.28, 124.52, 128.00, 130.73, 133.93, 136.72, 142.55, 146.80, 164.93, 173.74, 198.80. Anal. Calcd. For C₂₀H₁₉N₃O₃: C, 68.75; H, 5.48; N, 12.03. Found: C, 68.70; H, 5.50; N 12.02.

3, 7, 7-Trimethyl-5'-Chloro-7, 8-dihydro-1H-spiro [chromeno [2, 3-c] pyrazole- 4, 3'-indoline]-2', 5(6H)-diones (5b)

mp 215 °C (dec); IR (KBr): (vmax/cm⁻¹): 3207 (stretch NH), 3110 (stretch NH), 1706 (stretch CO), 1618 (stretch CO), 1473 (aromatic C=C), 806, 769 (C–Cl). ¹H NMR (DMSO-d₆, 400 MHz, δ ppm): 1.01 (6H, s, 2CH₃), 1.80 (3H, s, CH₃), 1.97–2.00 (2H, m, CH₂), 2.21–2.24 (2H, m, CH₂), 6.76 (1H, d, *J* = 8.0 Hz, CH), 7.12 (1H, d, *J* = 8.0 Hz, CH), 7.20 (1H, s, CH) 10.56 (1H, s, NH), 11.22 (1H, bs, NH). ¹³C NMR (100 MHz, DMSO-d₆, δ ppm): 11.14, 27.44, 30.55, 44.90, 48.12, 52.10, 97.84, 111.10, 120.13, 126.00, 128.63, 130.67, 135.90, 137.00, 141.33, 145.90, 164.34, 172.13, 197.00. Anal. Calcd For C₂₀ H₁₈Cl N₃O₃: C, 62.58; H, 4.73; N, 10.95. Found: C, 62.60; H, 4.75; N, 10.90.

3, 7, 7-Trimethyl-5'-Bromo-7, 8-dihydro-1H-spiro [chromeno [2, 3-c] pyrazole-4, 3'-indoline]-2', 5(6H)-diones (5c)

mp 185 °C (dec); IR (KBr): (vmax/cm⁻¹): 3216 (stretch NH), 3110 (stretch NH), 1724 (stretch CO), 1608 (stretch CO). ¹H NMR (DMSO-d₆, 400 MHz, δ ppm): 1.02

(6H, s, 2CH₃), 1.80 (s, 3H, CH₃), 1.97–2.06 (m, 2H, CH₂), 2.21–2.31 (m, 2H, CH₂), 6.72 (d, $J = 7.2$ Hz, 1H, CH), 7.25 (d, $J = 7.2$ Hz, 1H, CH), 7.32 (s, 1H, CH), 10.33 (s, 1H, NH), 11.58 (s, 1H, NH); ¹³C NMR (100 MHz, DMSO-d₆, δ ppm): 11.13, 25.33, 33.11, 44.80, 52.68, 97.85, 111.51, 120.28, 124.51, 125.99, 130.74, 133.93, 136.70, 142.56, 146.70, 164.74, 174.33, 197.00. Anal. Calcd. for C₂₀H₁₈BrN₃O₃: C, 56.09; H, 4.24; N, 9.81. Found: C, 56.06; H, 4.26; N, 9.90.

3, 7, 7-Trimethyl-5'-Nitro-7, 8-dihydro-1H-spiro [chromeno [2, 3-c] pyrazole-4, 3'-indoline]-2', 5-(6H) diones (5d)

mp 200 °C (dec); IR (KBr): ($\nu_{\text{max}}/\text{cm}^{-1}$): 3222 (stretch NH), 3104 (stretch NH), 1735 (stretch CO), 1604 (stretch CO), 1517 and 1336 (stretch N O). ¹H NMR (400 MHz, DMSO-d₆, δ , ppm): 1.05 (6H, s, 2CH₃), 1.80 (s, 3H, CH₃), 2.06–2.08 (m, 2H, CH₂), 2.26–2.28 (m, 2H, CH₂), 7.04 (d, $J = 8.4$ Hz, 1H, CH), 7.67 (s, 1H, CH), 8.13 (d, $J = 8.4$ Hz, 1H, CH), 10.18 (s, 1H, NH), 11.36 (s, 1H, NH); ¹³C NMR (100 MHz, DMSO-d₆): δ 11.11, 28.51, 32.16, 42.44, 46.83, 52.16, 97.88, 111.04, 119.41, 126.71, 137.25, 138.51, 144.16, 148.90, 164.02, 173.16, 198.90. Anal. Calcd. for C₂₀H₁₈N₄O₅: C, 60.91; H, 4.60; N, 14.21. Found: C, 60.89; H, 4.55; N, 14.30.

3, 7, 7-Trimethyl-5'-Methyl-7, 8-dihydro-1H-spiro [chromeno [2, 3-c] pyrazole-4, 3'-indoline]-2', 5(6H)-diones (5e)

mp 243 °C (dec); IR (KBr): ($\nu_{\text{max}}/\text{cm}^{-1}$): 3303 (stretch NH), 3191 (stretch NH), 1690 (stretch CO), 1625 (stretch CO). ¹H NMR (DMSO-d₆, 400 MHz, δ ppm): 0.94 (6H, s, 2CH₃), 1.72 (s, 3H, CH₃), 1.83 (s, 3H, CH₃), 1.98–2.13 (m, 2H, CH₂), 2.17–2.28 (m, 2H, CH₂), 6.90 (d, $J = 6.9$ Hz, 1H, CH), 7.13 (d, $J = 6.9$ Hz, 1H, CH), 7.48 (s, 1H, CH), 10.24 (s, 1H, NH), 10.78 (s, 1H, NH); ¹³C NMR (100 MHz, DMSO-d₆, δ ppm): 10.18, 27.42, 31.76, 32.91, 41.75, 55.68, 98.32, 108.33, 111.54, 121.49, 127.63, 129.48, 135.65, 139.47, 143.12, 145.96, 166.15, 173.35, 197.95. Anal. Calcd. For C₂₁H₂₁N₃O₃: C, 69.42; H, 5.78; N, 11.57. Found: C, 69.41; H, 5.80; N 11.53.

Results and discussion

Size distribution and surface morphology of Fe₃O₄, Fe₃O₄@SiO₂, Fe₃O₄@SiO₂-NH₂, and Fe₃O₄@SiO₂-SO₃H nanoparticles were investigated by SEM. As is shown in Fig. 2, SEM images of the samples indicate that the prepared nanoparticles have spherical shape and uniform size. It is observed that average size of Fe₃O₄@SiO₂-SO₃H and Fe₃O₄@SiO₂-NH₂ is about 19–33 and 25–31 nm, respectively.

XRD patterns of Fe₃O₄, Fe₃O₄@SiO₂-SO₃H, and Fe₃O₄@SiO₂-NH₂ are shown in Fig. 3. The characteristic peaks in the both spectra are in agreement with the standard XRD pattern of iron oxide (cubic phase). A broad peak in 2θ range of 19°–27° is related to the silica shell coated on Fe₃O₄ NPs. The crystallite size diameter (D) of both nanoparticles was calculated by Debye–Scherer equation:

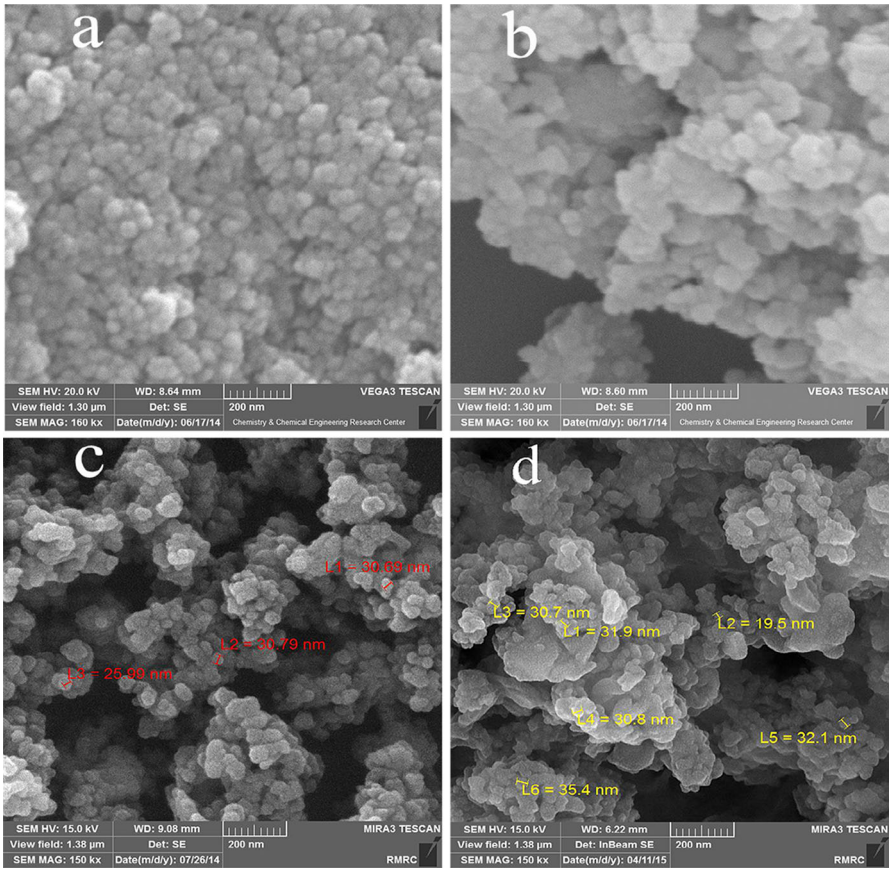


Fig. 2 SEM image of **a** Fe_3O_4 NPs, **b** $\text{Fe}_3\text{O}_4@SiO_2$ NPs, **c** $\text{Fe}_3\text{O}_4@SiO_2-NH_2$ NPs, and **d** $\text{Fe}_3\text{O}_4@SiO_2-SO_3H$

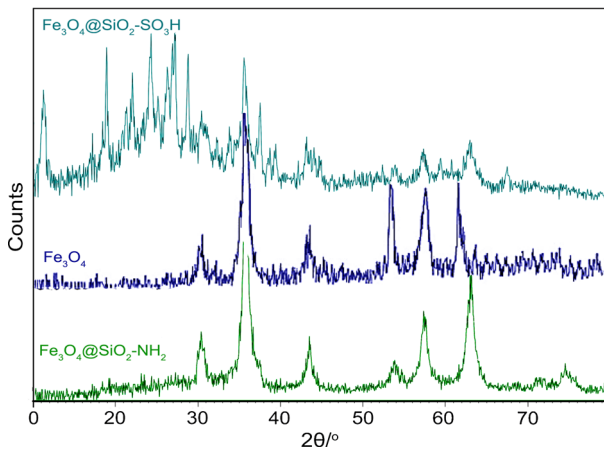


Fig. 3 The XRD pattern of $\text{Fe}_3\text{O}_4@SiO_2-SO_3H$, and XRD pattern of Fe_3O_4 and $\text{Fe}_3\text{O}_4@SiO_2-NH_2$

$$D = K\lambda/\beta \cos \theta$$

where λ is the X-ray wavelength (1.54 Å for Cu K α), θ is the Bragg angle of the maximum of diffraction peak, K is called the shape factor, which usually takes a constant value of about 0.9, and β is full-width at half-maximum (FWHM). The crystallite size of Fe₃O₄@SiO₂-SO₃H NPs calculated by Debye-Scherrer equation is about 23 nm that well agrees with the result shown by SEM. Also the crystallite size of Fe₃O₄@SiO₂-NH₂ NPs is obtained about 31 nm that well agrees with the result was shown by SEM.

Room temperature specific magnetization (M) versus applied magnetic field (H) curve measurements for Fe₃O₄, Fe₃O₄@SiO₂, Fe₃O₄@SiO₂-SO₃H, and Fe₃O₄@SiO₂-NH₂ are illustrated in Fig. 4.

The results demonstrate that all four samples are super paramagnetic and the highest saturation magnetization is 59.1 emu/g, which belongs to bare MNPs. As illustrated in Fig. 5, the amount of saturation magnetization for Fe₃O₄@SiO₂NPs, Fe₃O₄@SiO₂-SO₃H, and Fe₃O₄@SiO₂-NH₂ is 39.7, 10.43, and 31.7 emu/g, respectively. The lower saturation magnetization of Fe₃O₄@SiO₂-SO₃H and Fe₃O₄@SiO₂-NH₂ than that of Fe₃O₄@SiO₂NPs is attributed to the extra layer coated onto MNPs. However, it is still high enough to be separated by a magnet. These results prove that both catalysts can be easily separated and recovered by an external magnetic field.

The FT-IR spectra of sulfuric acid-functionalized Fe₃O₄@SiO₂, amino-functionalized Fe₃O₄@SiO₂, Fe₃O₄@SiO₂, and Fe₃O₄ NPs are shown in Fig. 5. The peak appeared at 580–600 cm⁻¹ in all the three spectra is related to characteristic absorption of Fe–O vibrations. The intense peaks appeared at around 1040–1080 cm⁻¹ are attributed to asymmetric and symmetric stretching vibrations of Si–O–Si bonds. These basic characteristic peaks verified that SiO₂ was coated on the surface of Fe₃O₄ NPs.

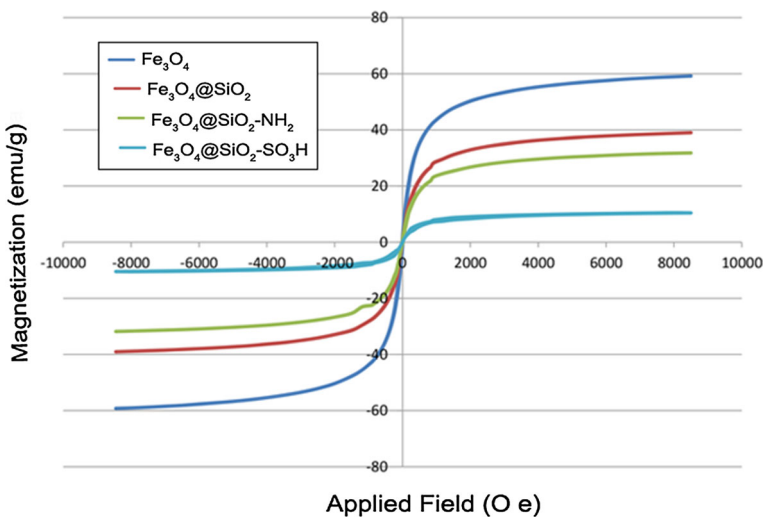


Fig. 4 The VSM curve of Fe₃O₄, Fe₃O₄@SiO₂, Fe₃O₄@SiO₂-NH₂, and Fe₃O₄@SiO₂-SO₃H

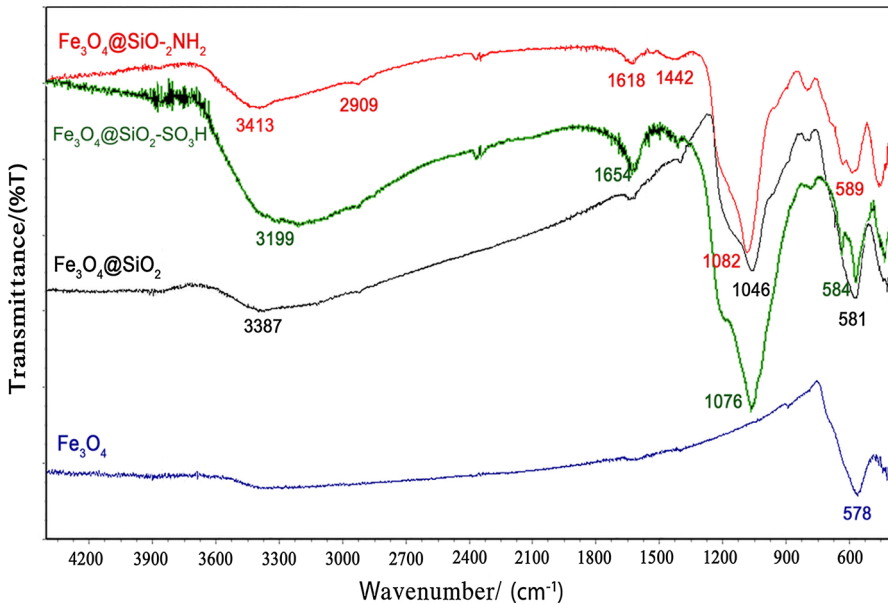


Fig. 5 FT-IR spectrum of Fe_3O_4 , $\text{Fe}_3\text{O}_4@SiO_2$, $\text{Fe}_3\text{O}_4@SiO_2-NH_2$, and $\text{Fe}_3\text{O}_4@SiO_2-SO_3H$ NPs

The FT-IR spectrum of amino-functionalized $\text{Fe}_3\text{O}_4@SiO_2$ shows the characteristic peaks at 1442 and 1618 cm^{-1} , which are related to the NH_2 bending and C–N stretching vibrations, respectively. Moreover, the peaks appeared at 2909 and 3413 cm^{-1} are attributed to stretching vibrations of C–H and N–H bonds, respectively, indicating $\text{Fe}_3\text{O}_4@SiO_2-NH_2$ NPs were successfully prepared. In the spectrum of $\text{Fe}_3\text{O}_4@SiO_2-SO_3H$, the presence of acid group is confirmed by the strong and broad peak at 3199 cm^{-1} , which can be attributed to OH stretching vibration. The presence of sulfonyl group is also verified by the peaks appeared at 1215 and 1120 cm^{-1} . The peak at 1120 cm^{-1} was covered with a stronger absorption peak of Si–O bond at 1076 cm^{-1} . These results reveal that the SO_3H groups were successfully adjoined the surface of $\text{Fe}_3\text{O}_4@SiO_2$ nanoparticles. Figure 6 shows the EDS spectra of $\text{Fe}_3\text{O}_4@SiO_2-SO_3H$ and $\text{Fe}_3\text{O}_4@SiO_2-NH_2$ NPs.

The presence of elements such as oxygen, iron, silicon, and sulfur was confirmed in the EDS spectrum of $\text{Fe}_3\text{O}_4@SiO_2-SO_3H$ NPs and their weight percentages were about 58.14, 22.77, 2.23, and 16.86, respectively. The elemental analysis of $\text{Fe}_3\text{O}_4@SiO_2-NH_2$ NPs indicated that the amounts of oxygen, carbon, iron, silicon, and nitrogen were about 46.83, 10.87, 26.26, 12.00, and 4.04 wt%, respectively. The results proved that amine and sulfonate groups were successfully coated onto the surface of MNPs.

Thermal behavior of the prepared catalysts was studied by TGA and the related curves are shown in Fig. 7. In the both curves, the small weight loss at temperatures between 30 and 250 $^{\circ}C$ is attributed to the removal of surface hydroxyl groups and physically adsorbed solvent molecules trapped in SiO_2 layer. The weight loss observed at 250–450 $^{\circ}C$ in TGA curve of $\text{Fe}_3\text{O}_4@SiO_2-SO_3H$ NPs is mainly related

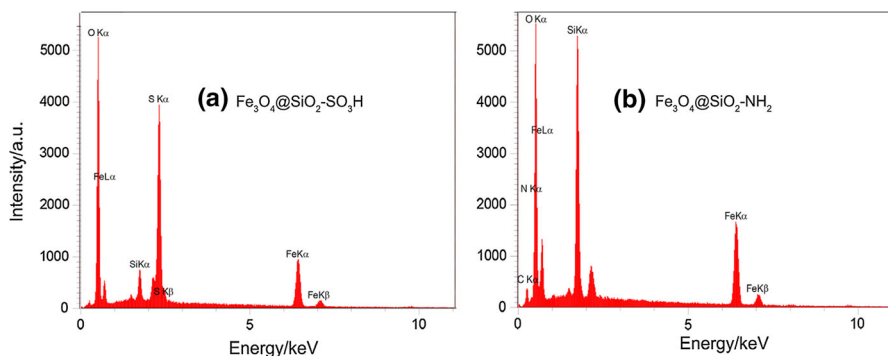


Fig. 6 a EDS spectrum of $\text{Fe}_3\text{O}_4@\text{SiO}_2\text{-SO}_3\text{H}$ NPs, b EDS spectrum of $\text{Fe}_3\text{O}_4@\text{SiO}_2\text{-NH}_2$ NPs

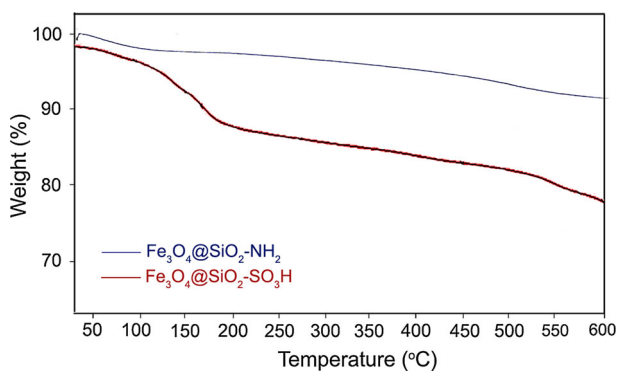


Fig. 7 TGA curve of $\text{Fe}_3\text{O}_4@\text{SiO}_2\text{-SO}_3\text{H}$ and $\text{Fe}_3\text{O}_4@\text{SiO}_2\text{-NH}_2$

to the decomposition of SO_3H groups grafted to the silica surface. Also, the weight loss at 250–450 °C in TGA curve of $\text{Fe}_3\text{O}_4@\text{SiO}_2\text{-NH}_2$ is due to the decomposition of APTES group attached to the silica surface. These results confirm that both catalysts are stable up to 200 °C and can be used in organic reactions.

After preparation and characterization of $\text{Fe}_3\text{O}_4@\text{SiO}_2\text{-SO}_3\text{H}$ and $\text{Fe}_3\text{O}_4@\text{SiO}_2\text{-NH}_2$ nanoparticles, their catalytic activities were investigated in a multicomponent reaction between dimedone, hydrazine hydrate, ethyl acetoacetate, and isatin as a model reaction. Initially, we selected various base catalysts such as L-proline, SSLP, and $\text{Fe}_3\text{O}_4@\text{SiO}_2\text{-NH}_2$ NPs and various acid catalysts such as p-TSA, Silica- SO_3H , sulfamic acid, and $\text{Fe}_3\text{O}_4@\text{SiO}_2\text{-SO}_3\text{H}$ NPs for the model reaction to compare their catalytic activity. The results were summarized in Table 1 and indicated that $\text{Fe}_3\text{O}_4@\text{SiO}_2\text{-SO}_3\text{H}$ NPs are the best catalysts considering yields of the product and reaction time. Moreover, the model reaction was performed in the presence of different amounts of catalyst. Also, the results clearly reveal that an increase in catalyst loading from 0.01 to 0.02 g improved the yield of the desired product to a great extent. The best results were obtained as 94 % yield within 0.5 h with the catalyst loading of 0.02 g (Entry 15).

Table 1 Optimization of reaction conditions using different catalysts

Entry	Catalyst	T/°C	Time (h)	Yield ^a (%)
1	None	80	5	Trace
2	L-proline (20 mol %)	80	1	80
3	SSLP (4.8 mol %)	80	1	90
4	Fe ₃ O ₄ @SiO ₂ -NH ₂ (0.01 g)	80	1	79
5	Fe ₃ O ₄ @SiO ₂ -NH ₂ (0.02 g)	80	1	92
6	Fe ₃ O ₄ @SiO ₂ -NH ₂ (0.03 g)	80	1	92
7	Fe ₃ O ₄ @SiO ₂ -NH ₂ (0.03 g)	60	1	74
8	Fe ₃ O ₄ @SiO ₂ -NH ₂ (0.03 g)	70	1	85
9	Fe ₃ O ₄ @SiO ₂ -NH ₂ (0.035 g)	80	1	92
10	p-TSA (0.05 g)	80	5	70
11	Silica-SO ₃ H (0.02 g)	80	2	83
12	Sulfamic acid (50 mol %)	80	0.5	81
13	Fe ₃ O ₄ @SiO ₂ -SO ₃ H (0.01 g)	80	0.5	78
14	Fe ₃ O ₄ @SiO ₂ -SO ₃ H (0.015 g)	80	0.5	85
15	Fe ₃ O ₄ @SiO ₂ -SO ₃ H (0.02 g)	80	0.5	94
16	Fe ₃ O ₄ @SiO ₂ -SO ₃ H (0.025 g)	80	0.5	94
17	Fe ₃ O ₄ @SiO ₂ -SO ₃ H (0.02 g)	70	0.5	86
18	Fe ₃ O ₄ @SiO ₂ -SO ₃ H (0.02 g)	60	0.5	76

^a Isolated yield**Table 2** Fe₃O₄@SiO₂-SO₃H nanoparticles catalyzed synthesis of spiro [chromeno [2, 3-c] pyrazole-4, 3'-indoline]-diones in various solvents in model reaction

Entry	Solvent	Time (min)	Yield ^a (%)
1	H ₂ O	30	75
2	EtOH	30	94
3	EtOH/H ₂ O (1:1)	30	86
4	CH ₃ CN	30	63
5	CH ₂ Cl ₂	30	Trace

^a Isolated yield

In another effort, the model reaction was carried out in different solvents such as H₂O, EtOH, CH₃CN, CH₂Cl₂, EtOH/H₂O (1:1), and the results are listed in Table 2. The reaction in CH₂Cl₂ has afforded the product in poor yields. It is observed that the reaction progress was appropriate in “EtOH,” and it was selected as the best solvent (Entry 2).

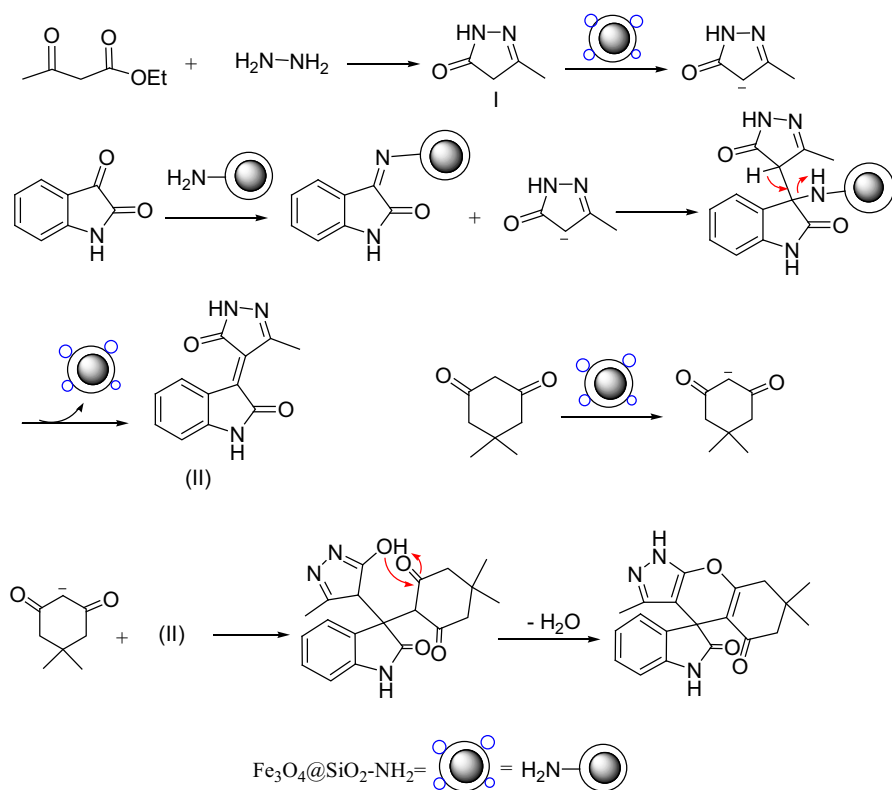
Using optimized conditions of solvent and catalyst obtained in previous sections, different spiro [chromeno [2, 3-c] pyrazole-4, 3'-indoline]-diones were synthesized through one-pot four-component reaction of various isatins, 1, 3-cyclohexadiones, ethyl acetoacetate, and hydrazine hydrate (Table 3). The results show that using isatin without substituent leads to higher yield than isatin having electron

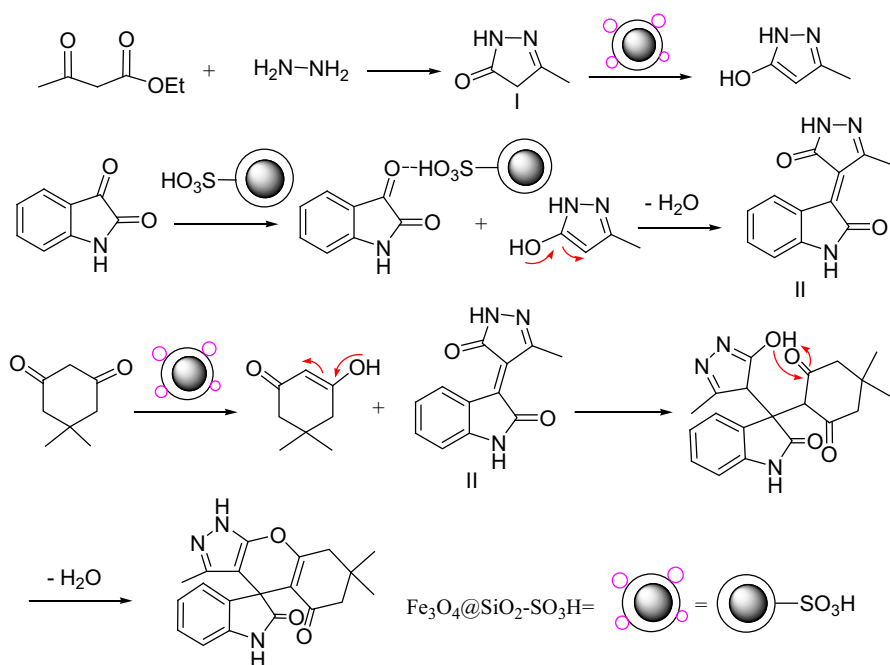
Table 3 One-pot synthesis of spiro [chromeno [2, 3-c] pyrazole-4, 3'-indoline]-diones catalyzed by $\text{Fe}_3\text{O}_4@\text{SiO}_2\text{-SO}_3\text{H}^{\text{a}}$ NPs

Entry	Product	R ₁	R	X	Time (min)	Yield ^b (%)	mp (°C) (dec)	mp (°C) [ref] (dec)
1	5a	H	Me	H	30	94	220	–
2	5b	H	Me	Cl	30	92	215	–
3	5c	H	Me	Br	30	89	185	–
4	5d	H	Me	NO ₂	30	87	200	–
5	5e	H	Me	Me	30	73	195	–
6	5f	Ph	H	H	30	85	308	312 [27]
7	5g	Ph	H	NO ₂	30	80	305	310 [27]
8	5h	Ph	Me	Br	30	87	241	244 [27]
9	5i	Ph	Me	NO ₂	30	85	307	315 [27]
10	5j	Ph	Me	H	30	91	240	243 [27]

^a Reaction conditions: isatin derivatives (1 mmol), ethyl acetoacetate (1.1 mmol), dimedone (1 mmol), hydrazine hydrate (1.1 mmol), and $\text{Fe}_3\text{O}_4@\text{SiO}_2\text{-SO}_3\text{H}$ NPs (0.02) g

^b Isolated yields

**Scheme 3** Proposed reaction pathway for the synthesis of spiro [chromeno [2, 3-c] pyrazole-4, 3'-indoline]-diones using $\text{Fe}_3\text{O}_4@\text{SiO}_2\text{-NH}_2$ NPs as catalyst



Scheme 4 Proposed reaction pathway for the synthesis of spiro [chromeno [2, 3-c] pyrazole-4, 3'-indoline]-diones using $\text{Fe}_3\text{O}_4@SiO_2-SO_3H$ NPs as catalyst

withdrawing groups (such as halides and nitro groups). Electron-donor substituents such as a methyl group decreased the yield of reaction. The electron-withdrawing substituents decreased the affinity of the carbonyl group in isatin to coordinate with the acidic hydrogen of $\text{Fe}_3\text{O}_4@SiO_2-SO_3H$ NPs. Also, it was shown that the yield of reaction with phenyl hydrazine was reduced compared to hydrazine hydrate because the intermediate (I) from phenyl hydrazine has lower affinity to condense with isatin via Knoevenagel reaction.

Enolization is catalyzed by acids and bases. A compound containing a carbonyl group with acidic α -hydrogen can be simply interconverted to enol form in the presence of acid or base catalysts. Two types of proposed mechanisms for this reaction are demonstrated in Schemes 3 and 4.

Scheme 3 shows a proposed mechanism for this reaction in the presence of $\text{Fe}_3\text{O}_4@SiO_2-NH_2$ NPs as a base catalyst. Initially hydrazine hydrate is reacted with 1, 3-dicarbonyl compound to form intermediate (I) via condensation reaction. Also, the carbonyl moiety in isatin is converted to imine group by the nucleophilic attack of $\text{Fe}_3\text{O}_4@SiO_2-NH_2$ to isatin. Secondly, intermediate (I) is condensed with isatin derivatives to form intermediate (II) via Knoevenagel condensation reaction. In the next step, dimedone reacts with intermediate (II) through Michael addition in the presence of $\text{Fe}_3\text{O}_4@SiO_2-NH_2$ NPs. Lastly, the final product is formed by intramolecular cyclization reactions. This proposed mechanism has also been supported by literature [28–30].

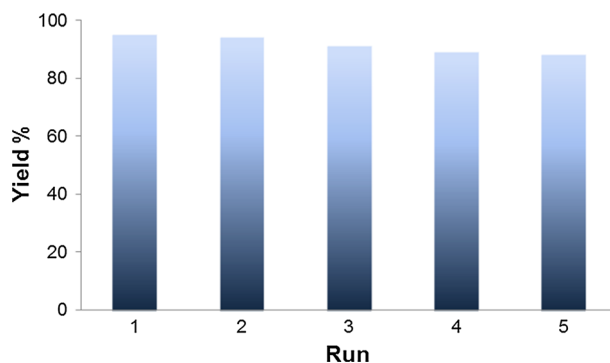


Fig. 8 Recyclability of $\text{Fe}_3\text{O}_4@\text{SiO}_2\text{-SO}_3\text{H}$ in the reaction

Scheme 4 shows a plausible mechanism for the synthesis of spiro [chromeno [2, 3-c] pyrazole-4, 3'-indoline]-diones in the presence of $\text{Fe}_3\text{O}_4@\text{SiO}_2\text{-SO}_3\text{H}$, as an acid catalyst. Initially, the reaction is started with the condensation reaction of 1, 3-dicarbonyl compound with hydrazine hydrate to form intermediate (I). The electrophilicity of the carbonyl group is increased by a strong coordinated bond formed between the carbonyl groups of isatin and $\text{Fe}_3\text{O}_4@\text{SiO}_2\text{-SO}_3\text{H}$ NPs. Afterward, intermediate (I) is rapidly condensed with the carbonyl group of the activated isatin to afford intermediate (II), which can be regarded as a fast Knoevenagel condensation reaction. Then, intermediate (II) reacts with dimedone through Michael addition. Finally, the intramolecular cyclization reactions followed by tautomerization afforded the corresponding product 5. The proposed mechanism is supported by the literature [27].

Reusability is one of the most significant properties of the prepared catalysts. The recyclability of MNPs- SO_3H was studied for the reaction of isatin, hydrazine hydrate, ethyl acetoacetate, and dimedone. After completion of the reaction, the nanocatalyst was easily separated using an external magnet. The recovered magnetic nanoparticles were washed several times with acetone and then dried at room temperature. Figure 8 indicates that the catalyst could be reused for the subsequent reaction without any noticeable loss of catalytic activity.

Conclusion

In summary, $\text{Fe}_3\text{O}_4@\text{SiO}_2\text{-NH}_2$ NPs and $\text{Fe}_3\text{O}_4@\text{SiO}_2\text{-SO}_3\text{H}$ NPs were employed respectively as a solid base and acid catalyst for the synthesis of spirooxindole containing chromene ring fragments in one-pot four-component reactions. $\text{Fe}_3\text{O}_4@\text{SiO}_2\text{-SO}_3\text{H}$ NPs have been selected as a better catalyst with respect to the yield of product and reaction times. This nanocatalyst was prepared simply and removed from the reaction mixtures by using an external magnetic field. Also, using this catalyst is more cost-effective compared to recently reported catalysts such as SSLP. Moreover, the products were obtained in excellent yields and short reaction times compared to using reported traditional acid catalysts such as p-TSA.

Acknowledgments The authors are grateful to department of chemistry, Science and Research branch, Islamic Azad University, Tehran, Iran for supporting this work.

References

1. X. Zheng, S. Luo, L. Zhang, J.P. Cheng, *Green Chem.* **11**, 455 (2009)
2. J. Deng, L.P. Mo, F.Y. Zhao, L.L. Hou, L. Yang, Z.H. Zhang, *Green Chem.* **13**, 2576 (2011)
3. P. Sharma, S. Rana, K.C. Barick, C. Kumar, H.G. Salunked, P.A. Hassan, *New J. Chem.* **38**, 5500 (2014)
4. L. Zeng, W. Ren, L. Xiang, J. Zheng, B. Chenb, A. Wu, *Nanoscale* **5**, 2107 (2013)
5. Y.M. Huh, Y.W. Jun, H.T. Song, S. Kim, J.S. Choi, J.H. Lee, S. Yoon, K.S. Kim, J.S. Shin, J.S. Suh, J. Cheon, *J. Am. Chem. Soc.* **127**, 12387 (2005)
6. J. Wang, S. Zheng, Y. Shao, J. Liu, Z. Xu, D. Zhu, *J. Colloid Interface Sci.* **349**, 293 (2010)
7. P.H. Li, B.L. Li, L.P. Mo, N. Liu, H.J. Kang, Y.N. Liu, Z.H. Zhang, *Appl. Catal. A Gen.* **457**, 34 (2013)
8. N.M. Mahmoodi, S. Khorramfar, F. Najafi, *Desalination* **279**, 61 (2011)
9. M.R. Nabid, Y. Bide, Z. Habibi, *RSC Adv.* **5**, 2258 (2015)
10. R.S. Shelkar, S.H. Gund, J.M. Nagarkar, *RSC Adv.* **4**, 53387 (2014)
11. H. Firouzabadi, N. Iranpoor, M. Gholinejad, J. Hoseini, *Adv. Synth. Catal.* **353**, 125 (2011)
12. V. Polshettiwar, R.S. Varma, *Tetrahedron* **66**, 1091 (2010)
13. R. Zhang, J. Liu, S. Wang, J. Niu, C. Xia, W. Sun, *ChemCatChem* **3**, 146 (2011)
14. F. Shi, M.K. Tse, S. Zhou, M.M. Pohl, J. Radnik, S. Hübner, K. Jähnisch, A. Brückner, M. Beller, *J. Am. Chem. Soc.* **131**, 1775 (2009)
15. H. Ghafari, A. Rashidizadeh, B. Ghorbani, M. Talebi, *New J. Chem.* **39**, 4821 (2015)
16. M. Li, W. Kong, L.-R. Wen, F.-H. Liu, *Tetrahedron* **68**, 4838 (2012)
17. S. Pal, M.N. Khan, S. Karamthulla, S.J. Abbas, L.H. Choudhury, *Tetrahedron Lett.* **54**, 5434 (2013)
18. M.C. Pirrung, K.D. Sarma, *J. Am. Chem. Soc.* **126**(2), 444 (2004)
19. A. Dömling, *Chem. Rev.* **106**, 17 (2006)
20. R.C. Larock, E.K. Yum, *J. Am. Chem. Soc.* **113**, 6689 (1991)
21. S. Kaladevi, J. Sridhar, B. Abhilashamole, S. Muthusubramanian, N. Bhuvanesh, *RSC Adv.* **4**, 34382 (2014)
22. R. Ghahremanzadeh, Z. Rashid, A.H. Zarnanic, H. Naeimi, *RSC Adv.* **4**, 43661 (2014)
23. M.A. Nasser, F. Kamali, B. Zakerinasab, *RSC Adv.* **5**, 26517 (2015)
24. J. Ganesan, J.B. Kothandapani, S.S. Nanubolub, Ganesan, *RSC Adv.* **5**, 28597 (2015)
25. C. Zou, S.Y. Chen, M. Leong, P.W. Ding, Smith, *Tetrahedron* **70**, 578 (2014)
26. F.Y. Miyake, K. Yakushijin, D.A. Horne, *Org. Lett.* **6**(5), 711 (2004)
27. R. Ghahremanzadeh, F. Fereshtehnejad, Z. Yasaei, T. Amanpour, A. Bazgir, *J. Heterocycl. Chem.* **47**, 967 (2010)
28. J. Feng, K. Ablajan, A. Sali, *Tetrahedron* **70**, 484 (2014)
29. R.Y. Guo, Z.M. An, L.P. Mo, S.T. Yang, S.X. Wang, Z.H. Zhang, *Tetrahedron* **69**, 9931 (2013)
30. Y. Zou, Y. Hu, H. Liu, D. Shi, *ACS Comb. Sci.* **14**, 38 (2012)
31. A. Khalafi-Nezhad, E.S. Shahidzadeh, S. Sarikhani, F. Panahi, *J. Mol. Catal. A Chem.* **379**, 1 (2013)